Characterization of ABS specimens produced via the 3D printing technology for drone structural components

Research Article **Open Access**

Carlo Giovanni Ferro, Salvatore Brischetto*, Roberto Torre, and Paolo Maggiore

Characterization of ABS specimens produced via the 3D printing technology for drone structural components

DOI 10.1515/cls-2016-0014
Received May 02, 2016; accepted May 03, 2016

Abstract: The Fused Deposition Modelling (FDM) technology is widely used in rapid prototyping. 3D printers for home desktop applications are usually employed to make non-structural objects. When the mechanical stresses are not excessive, this technology can also be successfully employed to produce structural objects, not only in prototyping stage but also in the realization of series pieces. The innovative idea of the present work is the application of this technology, implemented in a desktop 3D printer, to the realization of components for aeronautical use, especially for unmanned aerial systems. For this purpose, the paper is devoted to the statistical study of the performance of a desktop 3D printer to understand how the process performs and which are the boundary limits of acceptance. Mechanical and geometrical properties of ABS (Acrylonitrile Butadiene Styrene) specimens, such as tensile strength and stiffness, have been evaluated. ASTM 638 type specimens have been used. A capability analysis has been applied for both mechanical and dimensional performances. Statistically stable limits have been determined using experimentally collected data.

Keywords: Fused Deposition Modelling (FDM); 3D printing; mechanical properties; Acrylonitrile Butadiene Styrene (ABS); statistical process control

***Corresponding Author: Salvatore Brischetto:** Department of Mechanical and Aerospace Engineering, Politecnico di Torino, corso Duca degli Abruzzi, 24, 10129 Torino, Italy; Tel: +39.011.090.6813; Fax: +39.011.090.6899; Email: salvatore.brischetto@polito.it
Carlo Giovanni Ferro, Roberto Torre, Paolo Maggiore: Department of Mechanical and Aerospace Engineering, Politecnico di Torino, Turin, Italy

1 Introduction

Unmanned Aerial Vehicles (UAVs) are aircraft that can autonomously fly or can be remote controlled (Remotely Piloted Vehicle - RPV) [1]. During last years, the market of drones has rapidly grown [2] and these vehicles are used in many applications from package delivering to monitoring and farming. The distinguishing feature of the multirotor family is in their quadri- exa- or multi- copter configurations, depending on the number of used propellers. The innovative and patented solution proposed in [3] combines the advantage of flexibility (allowing different multicopter configurations changing the number of propellers and the geometry of the drone) with the low cost of the Fused Deposition Modelling (FDM) [4]. FDM is a typical additive manufacturing technology. A visual render of the proposed drone is presented in Figure 1. The flexibility allows to choose the optimal configuration depending on the mission profile and to set up the aircraft to optimize the mission. Further interesting UAV configurations are proposed in [5, 8]. However, the solution proposed in [3] remains one of the most advanced. The introduction of the additive manufacturing technology allows everyone to build and adapt the different versions of the drone at home just using a desktop 3D printer. The construction, part replacements and improvements in the main frame can be delivered with a distributed production system as suggested in [9]. In the preliminary project, ABS (Acrylonitrile Butadiene Styrene) was chosen as the structural material. However, it is necessary to understand the mechanical properties and the dimensional accuracy of specimens obtained via FDM. The mechanical properties are necessary to optimize the drone structure for the actual loads and material. This feature is necessary because the proportions of the ABS mix and the manufacturing process influence the mechanical properties of the finished pieces [10]. The dimensional accuracy is necessary to provide essential information on the tolerances to be taken into account. Nunez *et al.* [11] studied the dimensional accuracy in a commercial 3D-printer. However, this study must be

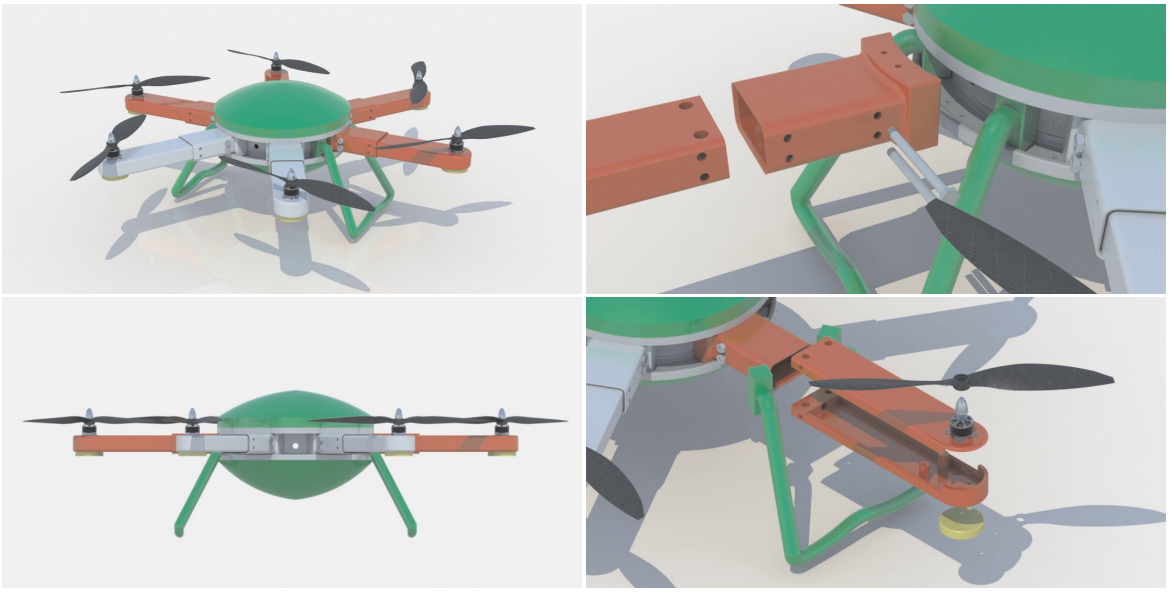

Figure 1: Renderings of several parts and details of the drone.

rearranged because the dimensional behavior is strictly dependent on the specific used 3D-printer. Furthermore, a capability study is set up to understand the statistical behaviour of 3D printers. Therefore, this paper is focused on both the mechanical and dimensional characterization and on the capability analysis based on the Six Sigma process.

1.1 The fused deposition modelling technology

The Additive Manufacturing (AM) has been developed to reduce the production costs and to increase the different typologies of vehicle that can be obtained directly from the end-user. This technique has been used together with the free shape topological optimization. Important savings in mass maintaining the same mechanical properties (stiffness, strength, etc.) have been obtained [12]. Nowadays, AM is one of the most promising manufacturing techniques [13]. The aim of the present work is to understand if this technique matches the structural and process requirements of the new UAV research and industrial development. FDM process starts with an approximation of the CAD model called STL (STereo Lithography) interface format. This format triangulates the component introducing an approximation by means of triangular facets [14, 15]. The errors introduced in this discretization are acceptable if they are under the accuracy level of the machine process (≃0.5mm). In addition to this feature, Zhang *et al.* [16] noted that in the case of very complex CAD models, the STL file could include various mistakes such as cracks, overlapping facets and so on. The STL file is the input for the CAM (Computer Aided Manufacturing) software [17], Slic3r in the present case, which generates the machining instructions [18] by horizontally slicing in equals sections the part with a height correspondent to the selected layer thickness (generally it is variable between 0.1mm and 0.3mm). The CAM automatically selects, for each layer, the path followed by the nozzle to build with stacks and taking as input some process variables (*e.g.*, stack width, air gab, stack angle). The process involves a polymeric filament of ABS, PLA (PolyLactic Acid) or Nylon [19, 20] which is semi-molted inside an extruder that moves in XY plane depositing a raster of material over the printing plane. These roads form the part depositing layer over layer. It is possible to build both the internal and the external faces with a minimal post processing. When the global path is finished, the platform moves towards the home position allowing the operator to extract the part. The produced parts have an anisotropic behavior, this feature was verified by Raut *et al.* [21]. The proposed characterization will just focus on the in-plane properties. Further developments to also characterize the properties along the other two axes will be proposed in a future companion paper.

2 Experimental procedure

The present experimental campaign considers specimens made of ABS printed with a home desktop Sharebot NG

printer with a single extruder. Printing operations are based on the FDM technology: a filament of raw material is heated and deposited in a semi-molten state on a glass surface. This feature guarantees that the new deposited material can merge with respect the material already present on the print floor. In its movements on the print floor, the nozzle follows a definite pattern depositing material along the perimeter and then deals with filling the interior. During the creation of the perimeter walls, the nozzle deposits a bead of material that faithfully follows the contour of the piece. During the filling of the interior, the nozzle follows a customizable pattern, which can be set choosing the so called fill pattern (*e.g.*, rectilinear, concentric, honeycomb) and the raster orientation. This procedure is repeated for each layer.

2.1 Specimen geometry

ASTM D638-10 [22] is the reference standard to determine the mechanical properties of plastic materials, reinforced or not, with a maximum limit for the thickness equal to 14mm. As a function of the maximum thickness, the standard provides 5 different types of test specimens, whose geometry and dimensions are well-defined. For the purposes of this study, 10 specimens of type V (which are those considered for a thickness under 4mm) were printed (see Figure 2). A drawing of the specimen is shown in Figure 3. The specimen is provided with expansions at the ends in order to allow a better gripping in the test machine. However, the test area of the specimen is restricted only to the narrow cross-sectional section.

2.2 Printing parameters

Various studies have been performed to determine how the print parameters affect the mechanical properties.

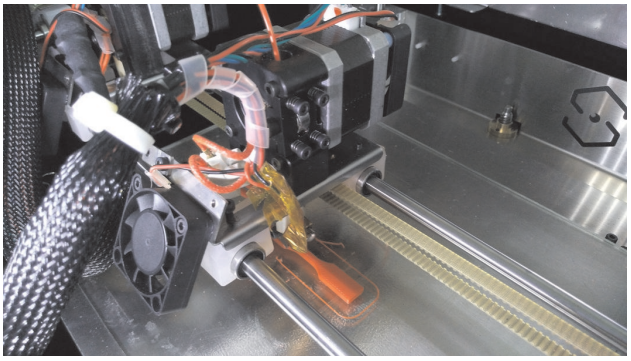

Figure 2: 3D printing process of a specimen.

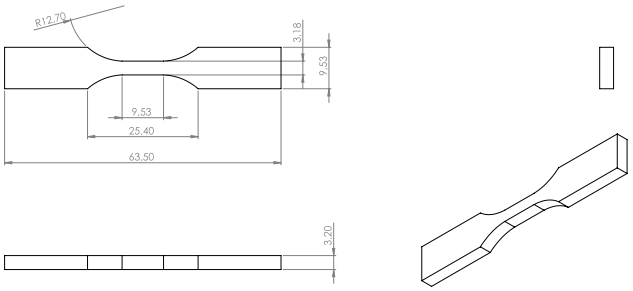

Figure 3: Sketch of the Type V ASTM D638 specimen.

Ahn *et al.* [23], Croccolo *et al.* [24] and Raunt *et al.* [21] identified the few ones that affect the properties of the FDM tecnology.

Bead/Raster width: the transverse dimension of the extruded bead, uniquely determined by the nozzle size. This parameter was therefore set according to the specifications of Sharebot NG, whose nozzle size is 0.35mm [25].

Air gap: the distance between two adjacent deposited beads. The range of allowable distances from negative values (overlapping beads) to positive values (not-in-contact beads). The choice of this value influences the density of the structure, as well as the printing time, because it has a direct influence on the amount of extruded material. Ahn *et al.* [23] noted that the lower the air gap is, the higher strength and stiffness are, being careful on the deposition of excess material which may degradate surface quality and dimensional tolerances. It is possible to specify the density of the internal infill. To preserve the results above mentioned, the maximum available value was set in the present work which means 100%.

Build temperature: the temperature at which the base material is brought to be extruded. It depends on the chosen material; the optimum extrusion temperatures for ABS are between 220°C and 250°C. Pincini [26] noted that the temperature influence on strength is negligible. An high extrusion temperature, equal to 245°C, has a significant and positive effect in stiffness. Therefore, a nozzle temperature of 245°C was set in the present work.

Raster orientation/angle: the orientation angle used for the various bead depositions, measured with respect to the building direction of the object. Criss-cross specimens were printed with a lamination of [45°/−45°].

Layer height: the vertical dimension of the extruded bead. It assumes a great importance as it determines the finish surface of the external walls (or of the internal ones, in hollow pieces). A height layer of 0.2mm was set in the present work.

Bed temperature: the temperature of the glass surface on which the piece is printed. Since ABS has the inclina-

tion to shrink and become deformed if cools too quickly, the print plan was heated to the maximum allowable temperature of 90°C [25].

Perimeters: how many perimeter walls will be printed. These peripheral beads faithfully follow the external and internal contours of the piece to be printed. Figure 4 shows the difference between a hypothetical specimen printed with three and two perimeter beads. In the case of the specimen with three peripheral beads, in the portion with smaller cross-sectional section, the printer is not able to fill the central area following the chosen Fill Pattern and Raster Orientation. Some trial run samples showed that this issue could cause stress-concentrating gaps in the connecting portion between the expansion and the useful length. For this reason only two peripheral beads were set in the present work.

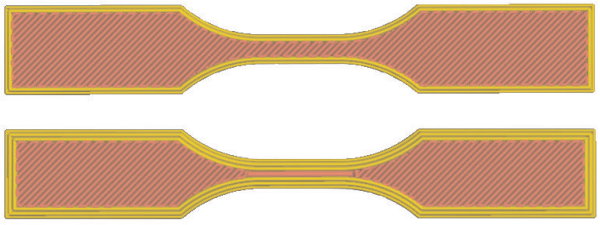

Figure 4: Specimens printed with two and three perimeter beads, respectively.

2.3 Test set-up

Each specimen was placed in the grips of a MTS QTEST 10 testing machine [27] (see Figure 5) being careful that the direction of application of the load coincides with the axis of the specimen. The machine can be controlled in position or in load, where the load is transmitted to the entire column and the absolute position is that of the upper jaw. The standard seen in [22] requires that the test takes place in velocity control and that the movable jaw moves with a constant speed. It is suggested to choose, for Type V specimens, the lowest speed, between the following cases, which produces rupture between 30s and 5min from the beginning of the test: 1±25% mm/min, 10±25% mm/min, 100±25% mm/min. However, the testing machine did not allow to set a speed lower than 10 mm/min, so the mentioned speed was used. The rupture occurred in a time included between 9.9s and 12.7s from the beginning of the test.

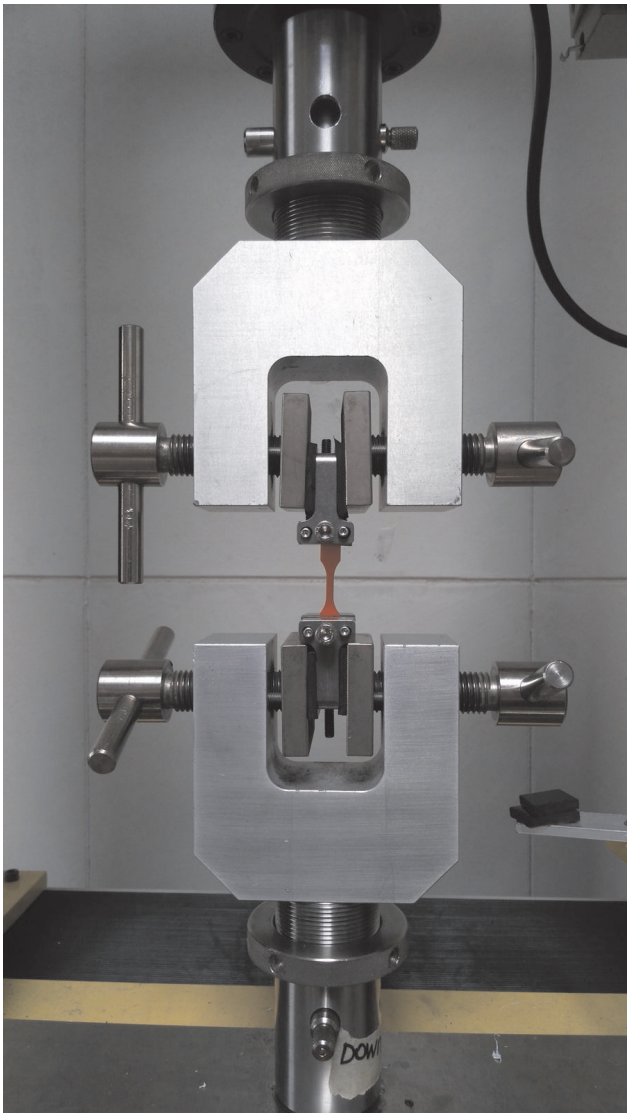

Figure 5: Artisan QTest10 testing machine during an experimental test.

3 Numerical analisys

The raw data plots are shown in Figures 6-9. The material is essentially fragile (see the image of the crossed-sectional section of the broken specimen of Figure 10), the common linear-elastic region is present. After a substantially linear trend of the stress-strain (σ-ϵ) curve, the proximity to the specimen failure is first heralded by laughable variations in the applied load with a further but limited deformation, and then underlined by a limited plastic region.

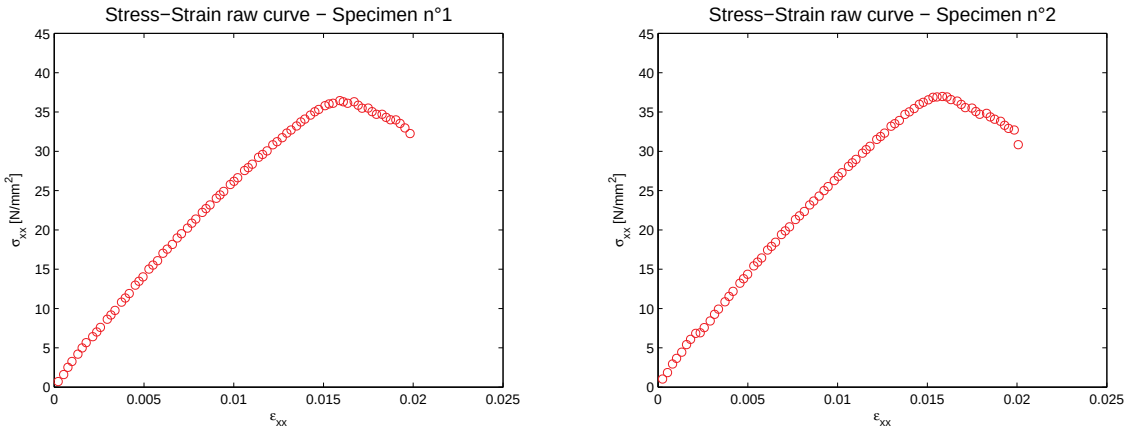

Figure 6: Raw stress-strain curve for specimens 1 and 2.

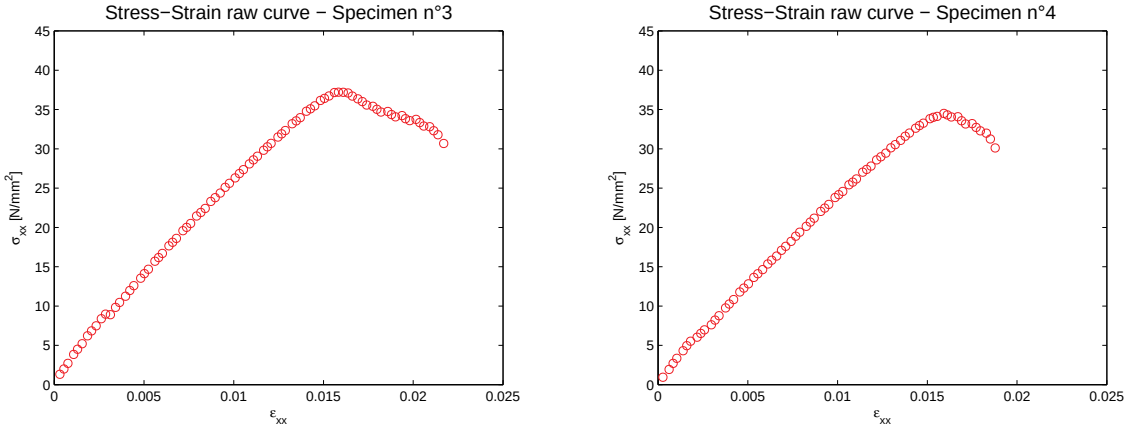

Figure 7: Raw stress-strain curve for specimens 3 and 4.

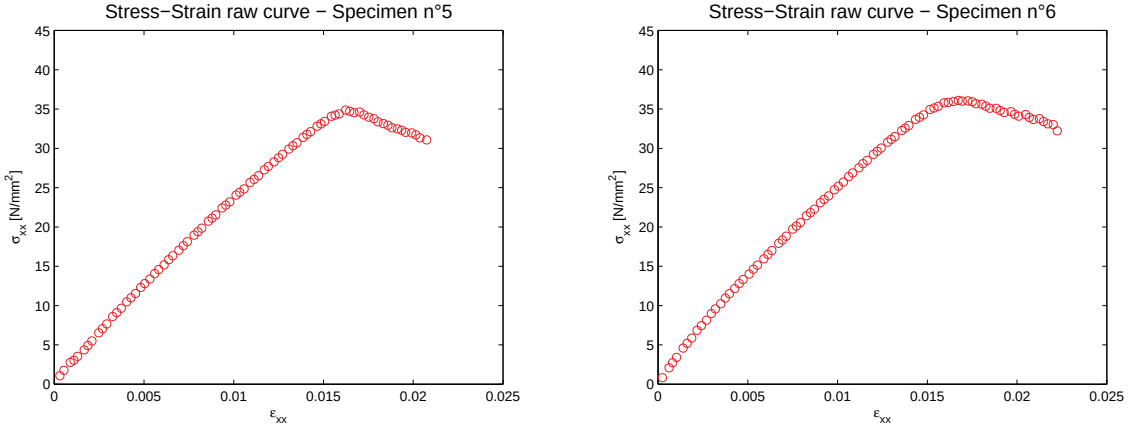

Figure 8: Raw stress-strain curve for specimens 5 and 6.

3.1 Post processing according to ASTM 638

For some of the 8 specimens, the curve presents two linear sections with slightly different slopes and spaced by a horizontal tangent point. This behavior required further studies. The first examined hypothesis could be a misalignment of the specimens and, at a certain load level, there was a slip of the expansions in the jaws with consequent alignment of the specimens to load application axis. This type of phenomenon is carefully described in annex A1.1

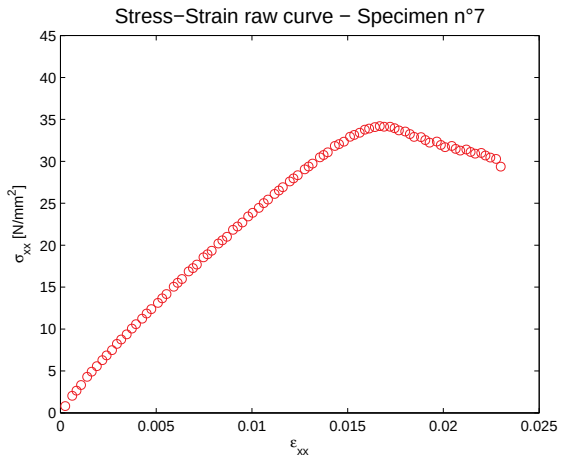

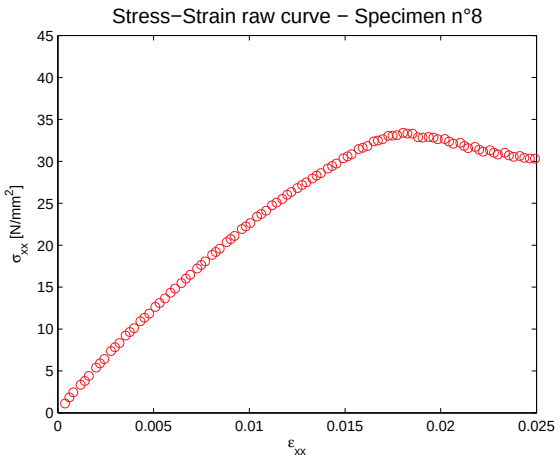

Figure 9: Raw stress-strain curve for specimens 7 and 8.

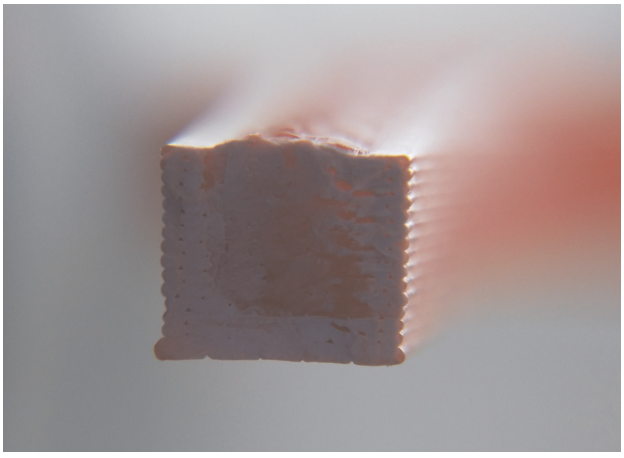

Figure 10: Crossed-sectional section of the broken specimen after the test.

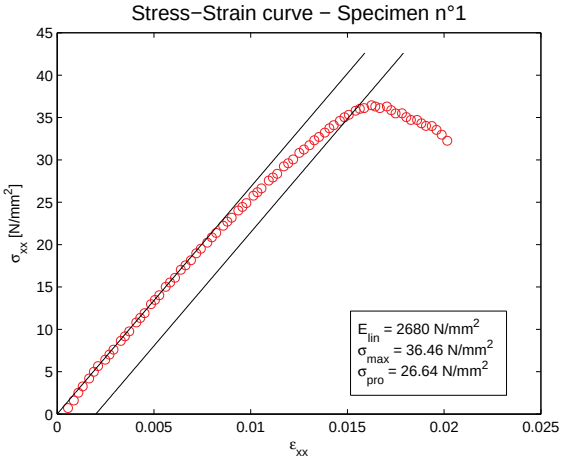

Figure 11: Actual stress-strain curve for specimen 1.

of ASTM638 [22]. It is emphasized by a typical stress-strain curve with a toe region which is an artifact caused by a take-up of slack and alignment or seating of the specimen. This region does not represent a property of the material. In order to obtain correct values of mechanical parameters this artifact must be compensated to give the corrected zero point on the strain or extension axis [22]. For materials exhibiting a region of linear behavior, a continuation of the linear region of the curve must be drown until the zero-stress is reached. This intersection of the straight line with the strain axis represents the corrected zero-strain point from which all strains must be measured. Hereafter, each derived mechanical property of ABS is presented, together with the employed calculation technique.

Modulus of Elasticity: a linear regression based on a gradually increasing range of values was made. Then, the coefficients of each linear regression were averaged. This previously exposed procedure was exclusively performed for the portion of the graph next to the change of slope.

Tensile Strength: the maximum load was divided by the original cross-sectional area in the narrow cross-sectional section.

Proportional Limit: being the greatest stress for which a material is capable of sustaining without any deviation from proportionality of stress-strain, it was conventionally identified as the value of stress at which the coefficient of the linear regression quoted above diverges more then the 5% from the found modulus of elasticity.

Taking into account what said in relation to the corrections to be applied on the linear portion of the stress-strain curve, the plots for each of the 8 specimens are presented in Figures 11-18. Table 1 gives the collected results.

Table 1: Mechanical experimental data for the eight specimens.

	Mechanical experimental data							
Specimen	1	2	3	4	5	6	7	8
E[MPa]	2680	2621	2470	2404	2351	2543	2372	2222
σ_{max}[MPa]	36.46	36.97	37.22	34.51	34.87	36.10	34.20	33.40
σ_{pro}[MPa]	26.64	28.97	33.20	27.81	30.33	23.95	25.44	26.01

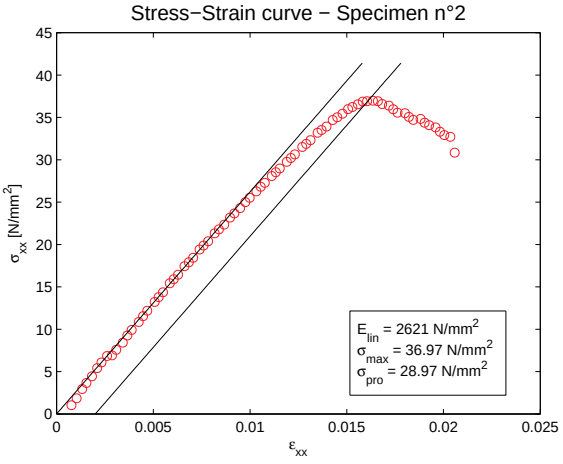

Figure 12: Actual stress-strain curve for specimen 2.

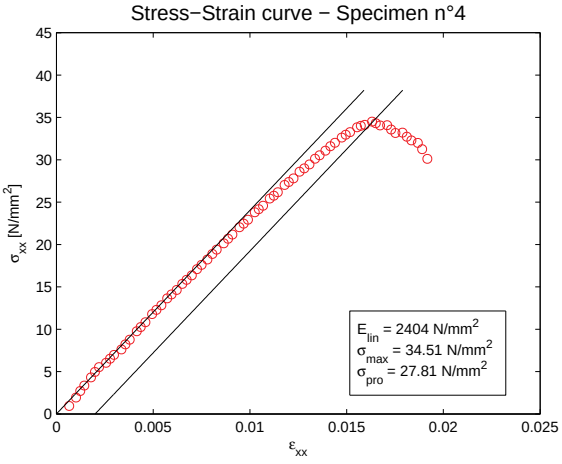

Figure 14: Actual stress-strain curve for specimen 4.

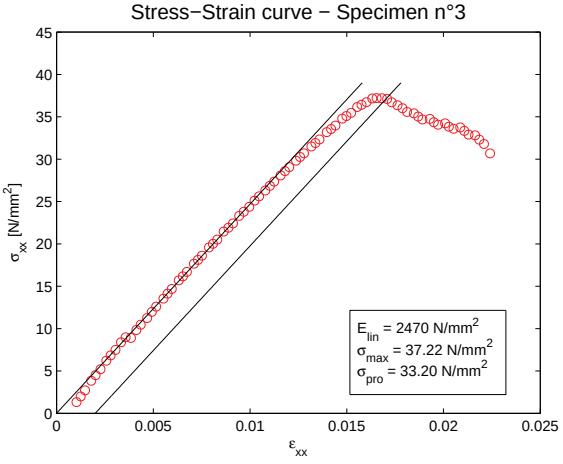

Figure 13: Actual stress-strain curve for specimen 3.

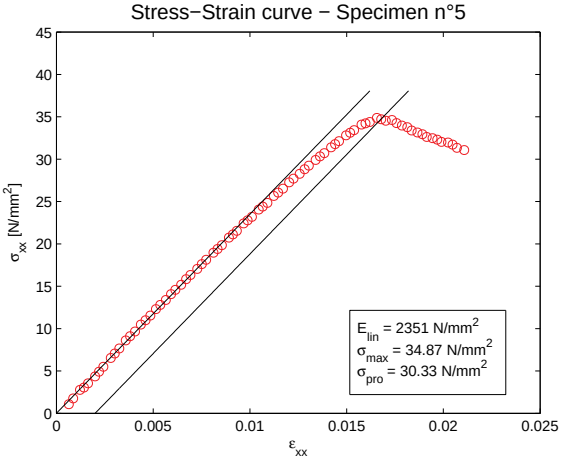

Figure 15: Actual stress-strain curve for specimen 5.

3.2 Statistical analysis

The capability analysis was applied to both mechanical and dimensional performances to determine the upper and lower limits delimiting in a statistically stable way the experimental collected values. The capability analysis goal is usually the reverse, it is used to determine if a process is able to produce results that meet project requirements. Here, the mechanical properties (and the geometrical ones, in the sense of the errors introduced in the printing process) are not known but they must be determined. This feature justifies the unconventional implementation of this process.

The distribution of many variables empirically approximates the shape of the normal distribution, so the experimentally obtained data were approximated with this theoretical distribution. The sample size is not so high, therefore it must be determined if the approximation is satisfac-

Table 2: Dimensional experimental data for the ten specimens.

Dimensional experimental data										
Specimen	1	2	3	4	5	6	7	8	9	10
Width[mm]	3.44	3.44	3.40	3.46	3.45	3.47	3.47	3.45	3.45	3.45
Length[mm]	62.90	62.94	62.91	62.98	62.88	62.91	62.99	63.02	63.04	62.95
Thickness[mm]	3.68	3.72	3.74	3.77	3.73	3.79	3.75	3.76	3.73	3.72
Weight[g]	1.58	1.61	1.60	1.61	1.57	1.62	1.62	1.60	1.61	1.61

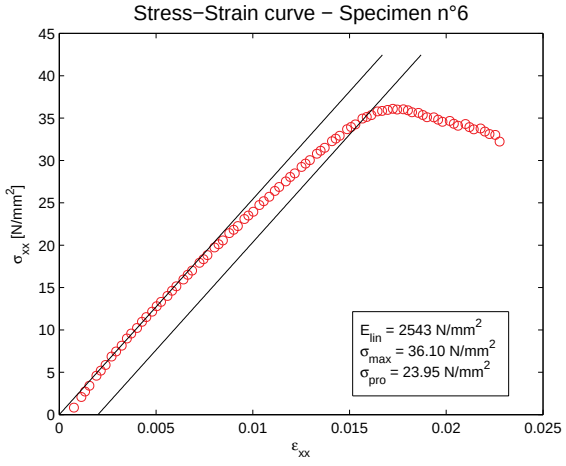

Figure 16: Actual stress-strain curve for specimen 6.

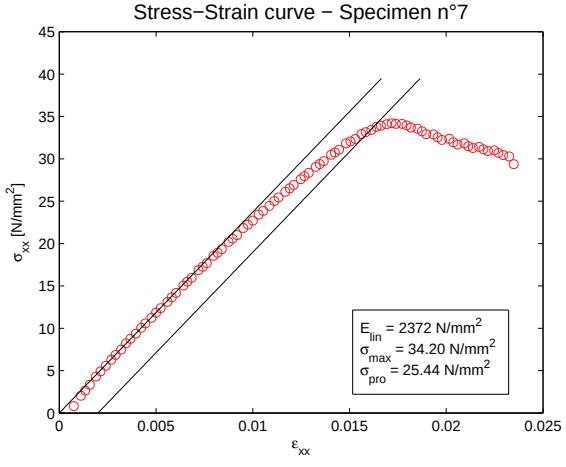

Figure 17: Actual stress-strain curve for specimen 7.

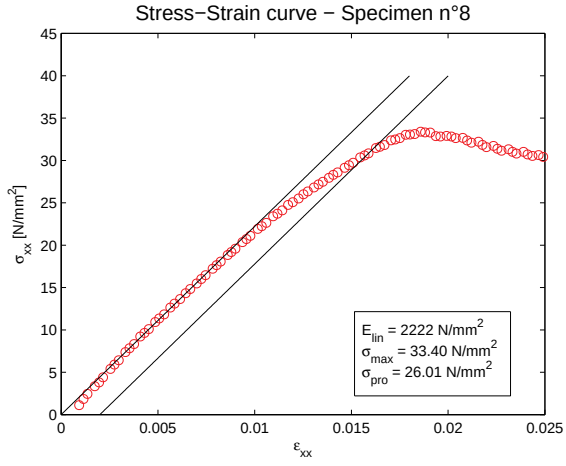

Figure 18: Actual stress-strain curve for specimen 8.

tory. Anderson and Darling [28, 29] proposed an hypothesis for tests usually employed to measure how well the data follow a particular distribution. This test is based on two indexes, commonly known as Anderson-Darling statistic (AD) and P-value indexes. For a specic set of data and distribution, the better fit is obtained for the smaller value of AD. However, it should be necessary that the AD of a particular distribution is substantially smaller than the AD of the others. The P-value is a probability index; small P-values provide strong evidence against the hypothesis that the data follow the specified distribution. This index is usually compared with a reference α value of 0.05 or 0.1. When P-value< α, it is excluded that the data come from the chosen distribution.

Tables 1 and 2 show the experimentally collected values; Tables 3-9 show the goodness of fit test for the seven experimental quantities investigated. There is no single distribution where the AD value is substantially smaller than the AD values of the other competing distributions. However, for the normal distribution, the Anderson-Darling statistics are always low and the P-value is considerably higher than the threshold value. Therefore, the normal distribution is considered a good fit. There is an exception, regarding the dimensional value studied in Table 3. An explanation can be found in the Section 4.1.1.

The Six Sigma is a set of techniques used for process improvement where the process quality is described in terms of the standard deviation $\hat{\sigma}$. The process data is usually collected in subgroups; the data within each subgroup usually refer to a short-term collection while the overall data refer to a longer collection. The sources of variability in the long and short term may be different. Therefore,

Table 3: Individual distribution identification for the width of specimens.

Goodness of fit test – Width		
	AD	**P-value**
Normal	0.722	0.040
Box-Cox Transformation	0.694	0.048
Lognormal	0.729	0.038
3-Parameter Lognormal	0.722	
Exponential	4.544	< 0.003
2-Parameter Exponential	2.195	< 0.010
Weibull	0.513	0.184
3-Parameter Weibull	0.513	0.108
Smallest Extreme Value	0.512	0.185
Largest Extreme Value	1.148	< 0.010
Gamma	0.727	0.060
3-Parameter Gamma	8.925	
Logistic	0.547	0.103
Loglogistic	0.550	0.100
3-Parameter Loglogistic	0.547	
Johnson Transformation	0.490	0.168

Table 4: Individual distribution identification for the length of specimens.

Goodness of fit test - Length		
	AD	**P-value**
Normal	0.254	0.648
Box-Cox Transformation	0.253	0.652
Lognormal	0.254	0.649
3-Parameter Lognormal	0.266	
Exponential	4.579	< 0.003
2-Parameter Exponential	0.485	> 0.250
Weibull	0.369	> 0.250
3-Parameter Weibull	0.257	> 0.500
Smallest Extreme Value	0.369	> 0.250
Largest Extreme Value	0.253	> 0.250
Gamma	0.292	> 0.250
3-Parameter Gamma	0.296	
Logistic	0.284	> 0.250
Loglogistic	0.284	> 0.250
3-Parameter Loglogistic	0.272	

the indices used to identify the natural variations experienced by a process may assume different values. The most common indices are defined as [30]:

$$\hat{P}_{pk} = min(\frac{USL - \hat{\mu}}{3\hat{\sigma}_p}, \frac{\hat{\mu} - LSL}{3\hat{\sigma}_p}); \quad (1)$$
$$\hat{C}_{pk} = min(\frac{USL - \hat{\mu}}{3\hat{\sigma}_{R/d_2}}, \frac{\hat{\mu} - LSL}{3\hat{\sigma}_{R/d_2}})$$

Table 5: Individual distribution identification for the thickness of specimens.

Goodness of fit test - Thickness		
	AD	**P-value**
Normal	0.203	0.828
Box-Cox Transformation	0.199	0.840
Lognormal	0.205	0.823
3-Parameter Lognormal	0.207	
Exponential	4.519	< 0.003
2-Parameter Exponential	1.437	< 0.010
Weibull	0.274	> 0.250
3-Parameter Weibull	0.212	> 0.500
Smallest Extreme Value	0.278	> 0.250
Largest Extreme Value	0.397	> 0.250
Gamma	0.207	> 0.250
3-Parameter Gamma	2.579	
Logistic	0.187	> 0.250
Loglogistic	0.187	> 0.250
3-Parameter Loglogistic	0.187	

where USL is the Upper Specification Limit, LSL is the Lower Specification Limit, $\hat{\mu}$ is the overall average, $\hat{\sigma}_p$ is the sample standard deviation and $\hat{\sigma}_{R/d_2}$ is an estimate of the process standard deviation using the subgroup ranges R_i (with i=1,...,m).

The first index in eq.(1) is a Process Performance index. The second one is a Process Capability index. The mathematical expressions seem identical and the only difference is the estimate of the process standard deviation. In the Process Capability, the standard deviation is calculated using only the variability within each subgroup. In the Process Performance all the data are combined, therefore both the within and the between subgroup variability are used. The Process Performance should be studied when a process is too new to determine whether it is in statistical control. The Process Capability can be studied when a process is stable and in statistical control. Theoretically when $C_{pk} > P_{pk}$, it is more likely that in the short term the process is stabler. The inverse may happen in special cases, such as a small data sample size.

In the Six Sigma method, the sigma value of a process (sigma level) represents the number of standard deviations that it is possible to measure between the central value and the closest tolerance limit. A $\hat{\sigma}$ level equals 4 has been used and it allows a process yield of 99.38%.

Table 6: Individual distribution identification for the weight of specimens.

Goodness of fit test - Weight		
	AD	**P-value**
Normal	0.543	0.119
Box-Cox Transformation	0.513	0.145
Lognormal	0.551	0.116
3-Parameter Lognormal	0.578	
Exponential	4.507	< 0.003
2-Parameter Exponential	1.453	< 0.010
Weibull	0.357	> 0.250
3-Parameter Weibull	0.352	0.355
Smallest Extreme Value	0.352	> 0.250
Largest Extreme Value	0.782	0.034
Gamma	0.583	0.145
3-Parameter Gamma	3.218	
Logistic	0.504	0.150
Loglogistic	0.511	0.143
3-Parameter Loglogistic	0.504	

Table 7: Individual distribution identification for the ABS Young Modulus E.

Goodness of fit test - E ABS		
	AD	**P-value**
Normal	0.160	0.915
Box-Cox Transformation	0.174	0.890
Lognormal	0.156	0.922
3-Parameter Lognormal	0.182	
Exponential	3.268	< 0.003
2-Parameter Exponential	0.757	0.085
Weibull	0.236	> 0.250
3-Parameter Weibull	0.186	> 0.500
Smallest Extreme Value	0.255	> 0.250
Largest Extreme Value	0.202	> 0.250
Gamma	0.182	> 0.250
3-Parameter Gamma	0.919	
Logistic	0.185	> 0.250
Loglogistic	0.180	> 0.250
3-Parameter Loglogistic	0.178	

Table 8: Individual distribution identification for the ABS maximum stress σ_{max}.

Goodness of fit test – σ_{max} ABS		
	AD	**P-value**
Normal	0.277	0.549
Box-Cox Transformation	0.277	0.549
Lognormal	0.277	0.550
3-Parameter Lognormal	0.328	
Exponential	3.408	< 0.003
2-Parameter Exponential	0.643	0.133
Weibull	0.336	> 0.250
3-Parameter Weibull	0.331	0.491
Smallest Extreme Value	0.337	> 0.250
Largest Extreme Value	0.314	> 0.250
Gamma	0.327	> 0.250
3-Parameter Gamma	0.820	
Logistic	0.320	> 0.250
Loglogistic	0.321	> 0.250
3-Parameter Loglogistic	0.321	

Table 9: Individual distribution identification for the ABS proportional stress σ_{pro}.

Goodness of fit test - σ_{pro} ABS		
	AD	**P-value**
Normal	0.192	0.845
Box-Cox Transformation	0.118	0.981
Lognormal	0.151	0.932
3-Parameter Lognormal	0.122	
Exponential	3.003	< 0.003
2-Parameter Exponential	0.444	> 0.250
Weibull	0.311	> 0.250
3-Parameter Weibull	0.175	> 0.500
Smallest Extreme Value	0.379	> 0.250
Largest Extreme Value	0.123	> 0.250
Gamma	0.181	> 0.250
3-Parameter Gamma	0.245	
Logistic	0.182	> 0.250
Loglogistic	0.155	> 0.250
3-Parameter Loglogistic	0.122	

4 Results

The results collected from the capability analysis are presented in two different sections: the dimensional properties of the specimens and their behaviour as index of process stability for non-functional prototypes and the mechanical capability analysis for functional prototypes.

4.1 Capability analysis on dimensional values

As a precondition, the goodness of fit test was carried out to verify if the normal distribution could be used to study the distribution of the experimentally collected values. In the present cases, the software Minitab was used [31]. Three characteristics have been taken into account as

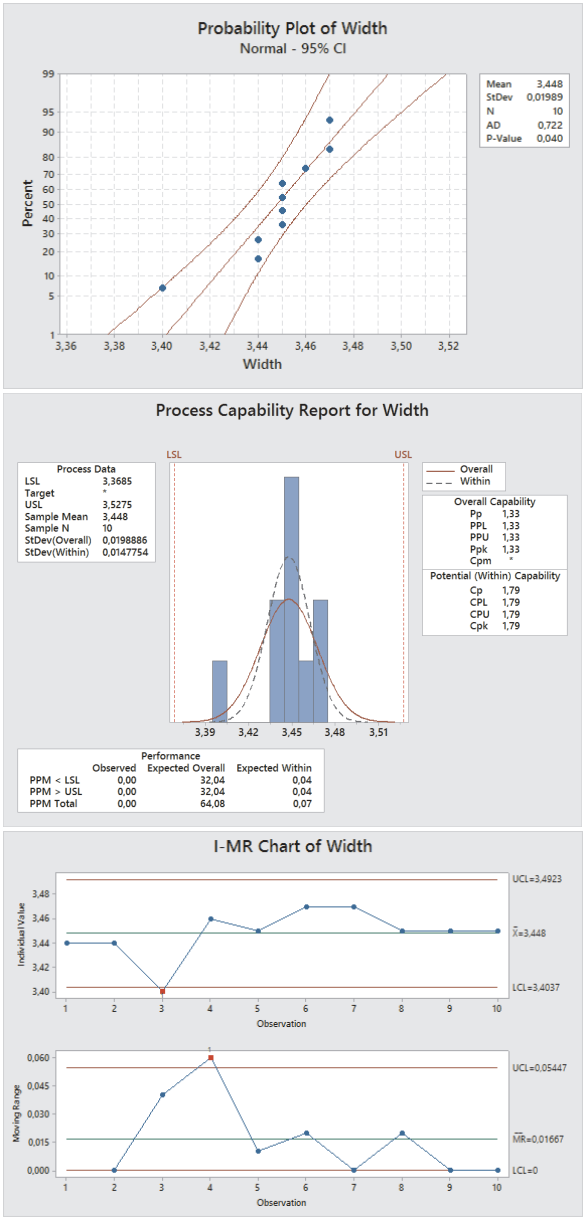

Figure 19: Probability Plot, Process Capability Report and I-MR Chart for the width of specimens.

significative for the dimensional measurements: the central width and thickness of the specimen, and its overall length. These values have been chosen because they are indexes of how the printer performs along the three main axes of construction. The sample was composed by 10 specimens; the collected results are reported in Table 2.

4.1.1 Central width

As a first step in the analysis of the results, the Probability Plot is presented in Figure 19. This plot allows to evaluate the fit of the normal distribution to the collected data and to extrapolate some preliminary conclusions. It can be seen that the average value of the measured width at the central zone is equal to 3.448mm, while the nominal value was 3.18mm. This feature means that the machine builds parts in average wider of 0.26mm, which represent an average error of 8%. This difference could be due to the extrusion process that, not yet considering with sufficient precision the diameter of the raster, underestimates it. The standard deviation calculated on the total sample is equal to 0.020. The Anderson-Darling statistic is not so low, being equal to 0.722 and the P-value is lower than the threshold value. The normal distribution seems not to be a good fit for the collected data. The data do not follow a straight line. However, this distribution was all the same used because, being one point remarked outside of the control chart, an error in measurement probably happened. In Figure 19 the Process Capability Report is presented. It was necessary to identify those upper and lower limits which guaranteed that the percentage corresponding to a Sigma Level of 4 would have fallen within that range. These were identified by imposing a P_{pk} (rather than a C_{pk}) equal to 1.33. This approach is more conservative since it allows to take into account the long term variability, statistically more marked than the short term one. As indicated, the lower limit for the interval corresponding to the Sigma Level 4, centered on the mean value, is equal to 3.3685mm while the upper limit is equal to 3.5275mm. Being the nominal value outside this range, those limits indicate that at least the 99.38% of the specimens will have a higher value of width compared to the one designed into the CAD. This overvalue can be corrected passing through the CAM process and adding a re-scaling factor. The control chart in Figure 19 allows to say that, except for the specimen number 3, the process is stable and inside of the boundaries. For this measure, it is advisable to repeat it with a new sample to evaluate if it was an error of measurement.

4.1.2 Overall lenght

The second measurement presented concerns the overall length of the Type V specimen [22]. The nominal value for this measure is 63.5mm. In the Probability Plot of Figure 20 the found average value equals 62.95mm. The average error of 0.55mm shows a percentage defect in length of 1%. Together with what found earlier, this can be taken into account in the CAM phase rescaling all the parts in X of the 8% and in Y of the -1%. The standard deviation of this sample of measurement is 0.05; since the AD value is considerably low, being equal to 0.254, and the p-value, equal to

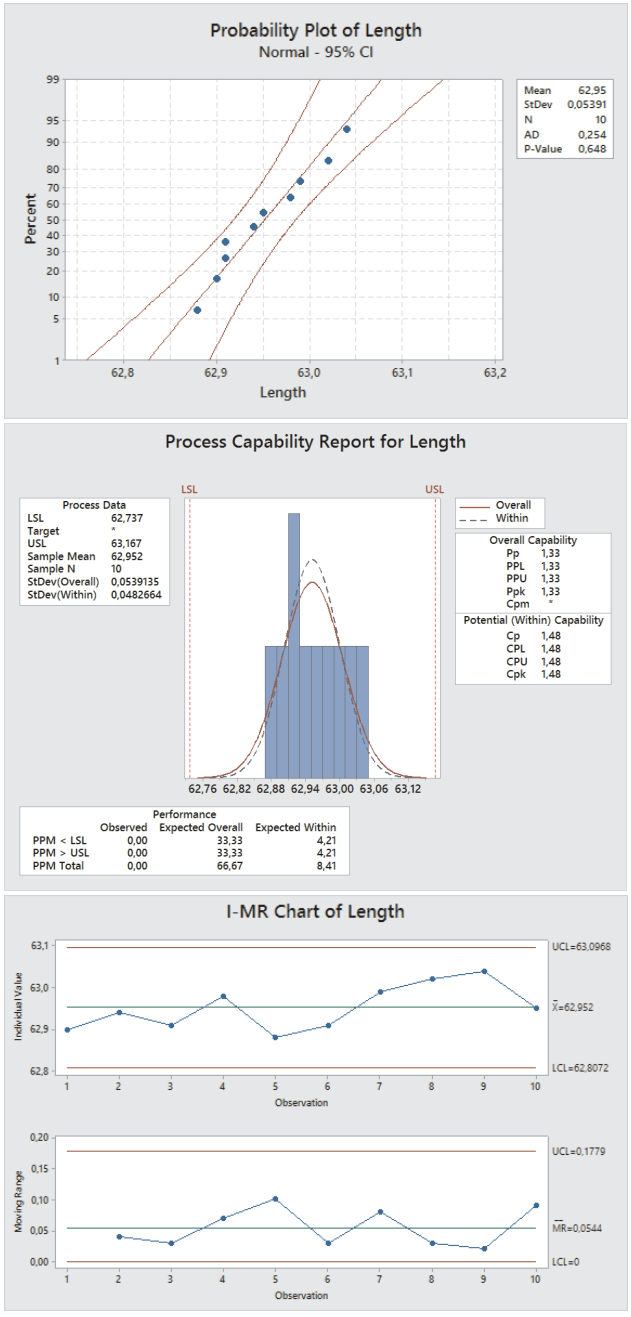

Figure 20: Probability Plot, Process Capability Report and I-MR Chart for the length of specimens.

0.648, is considerably higher than the threshold one, the gaussian approximation seems to be acceptable. The capability histogram in Figure 20 shows a equally spaced distribution; taking into account what said in relations to the Sigma Level, the lower limit was identified as 62.737mm, while the upper limit is 63.167mm. Neither of the tested specimens reached the nominal value of 63.5mm. The proposed boundaries lead to a P_{pk} index of 1.33. Finally, the control chart in Figure 20 shows a globally stable process, not conditioned from particular external effects.

Summing up, it can be said that the in-plane dimensions have a stable and controlled performance. The real values are not centered in the nominal ones, therefore a scale effect must be taken into account when the g-code is produced.

4.1.3 Central thickness

The last investigation for the dimensional parameters refers to the out-of-plane length of the specimens (the thickness). The designed value according to Figure 3 was 3.2mm, while in Figure 21 it can be seen that the average value exceeds with an average of 3.74mm. This phenomenon has a scale and a side effect which need to be taken into account: while preparing the g-code, the CAM slicer adds a first expendable layer of 0.3mm to preserve the part from the plate effect (mis-attachment, distortion, etc). Therefore, the effective error in z direction will be 0.24mm, representing the 7.5%. With a standard deviation of 0.203, a p-value of 0.828 and a quasi-linear distribution over the Figure 21, the distribution can be considered normal. For what concerns the Capability Histogram chart, Figure 21 shows that the samples are centered along the mean; to be congruent with the Sigma Level chosen, the lower and upper boundaries are 3.616mm and 3.862mm respectively, leading to a P_{pk} index of 1.33. The control chart reported in Figure 21 shows that the process performs always inside the limits with a random trend.

4.1.4 Weight

In addition to the Capability Analysis made on dimensional characteristics, a study on the weight of specimens was performed to understand how the quantity of the extruded material varied. Taking into account the volume of the specimen to be printed equal to 1527.28mm^3 and the density of the ABS filament declared by the vendor equal to 0.0011g/mm^3, a weight of 1.6808g was expected. However, as shown by the Normal Probability Plot in Figure 22, an average value of 1.603g was found. Taking into account a Sigma Level of 4, the Capability Histogram in Figure 22 shows that the boundary limits which grants a P_{pk} of 1.33 are 1.5333g and 1.6733g. This figure indicates that in more than the 99.38% of the printing processes the quantity of material to be extruded is understimated. The control chart in Figure 22 shows a quite randomic trend that will need more specimens to be completely clarified.

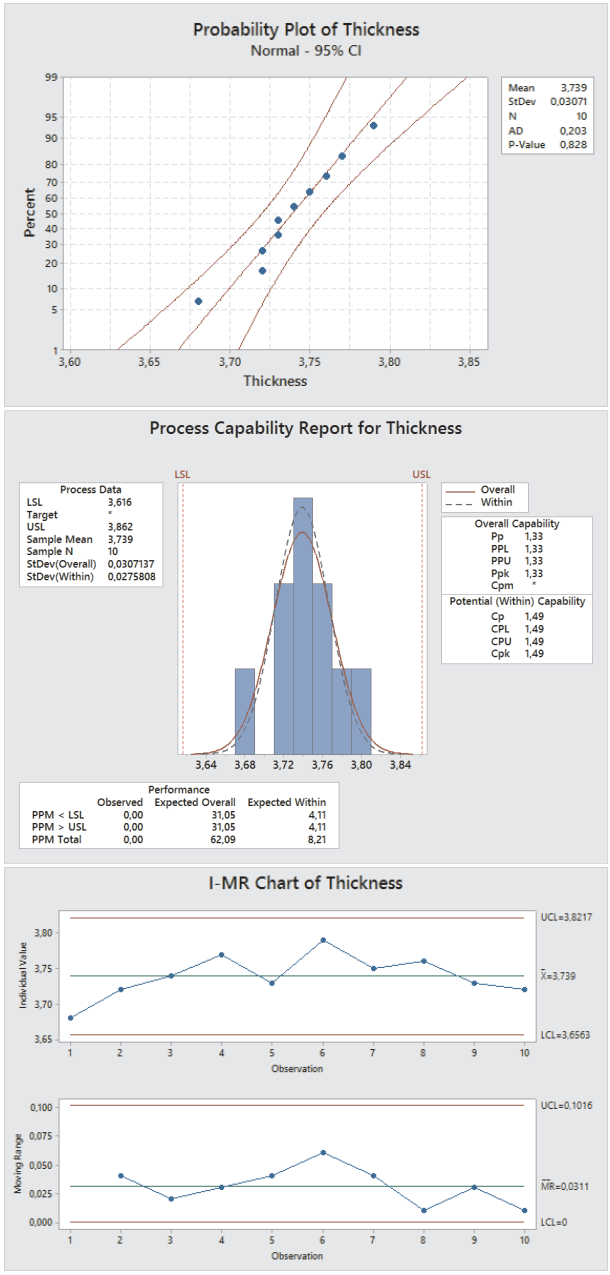

Figure 21: Probability Plot, Process Capability Report and I-MR Chart for the thickness of specimens.

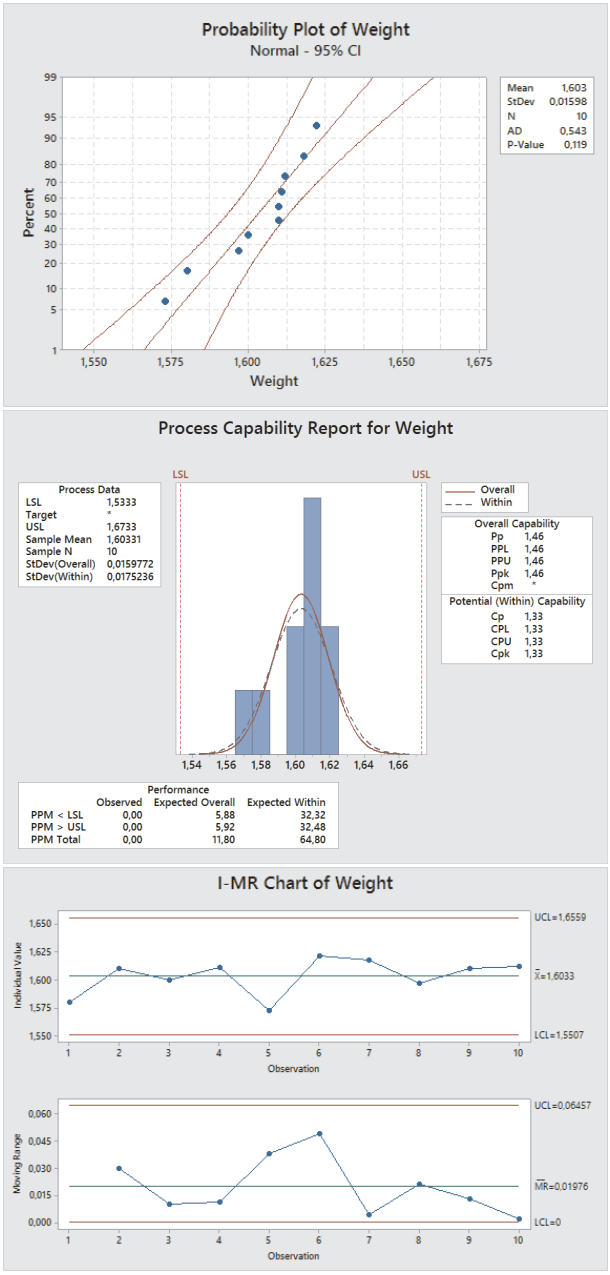

Figure 22: Probability Plot, Process Capability Report and I-MR Chart for the weight of specimens.

4.2 Capability analysis on mechanical properties

In this sections the statistical analysis for the mechanical properties of the tested specimens is reported. Among the 10 produced specimens, two specimens failed the test due to misalignment; the values will be therefore referred to 8 samples. Three values have been taken into account as significative: Young modulus (E), maximum stress at rupture (σ_{max}) and stress at proportional limit (σ_{pro}). For each of these characteristics, the control chart, the probability plot and the capability analysis are presented, together with the most important results. The collected values are reported in Table 1.

4.2.1 Young Modulus

The experimental values reported in Table 1 are the basis for the capability analysis. The first graph presented in Fig-

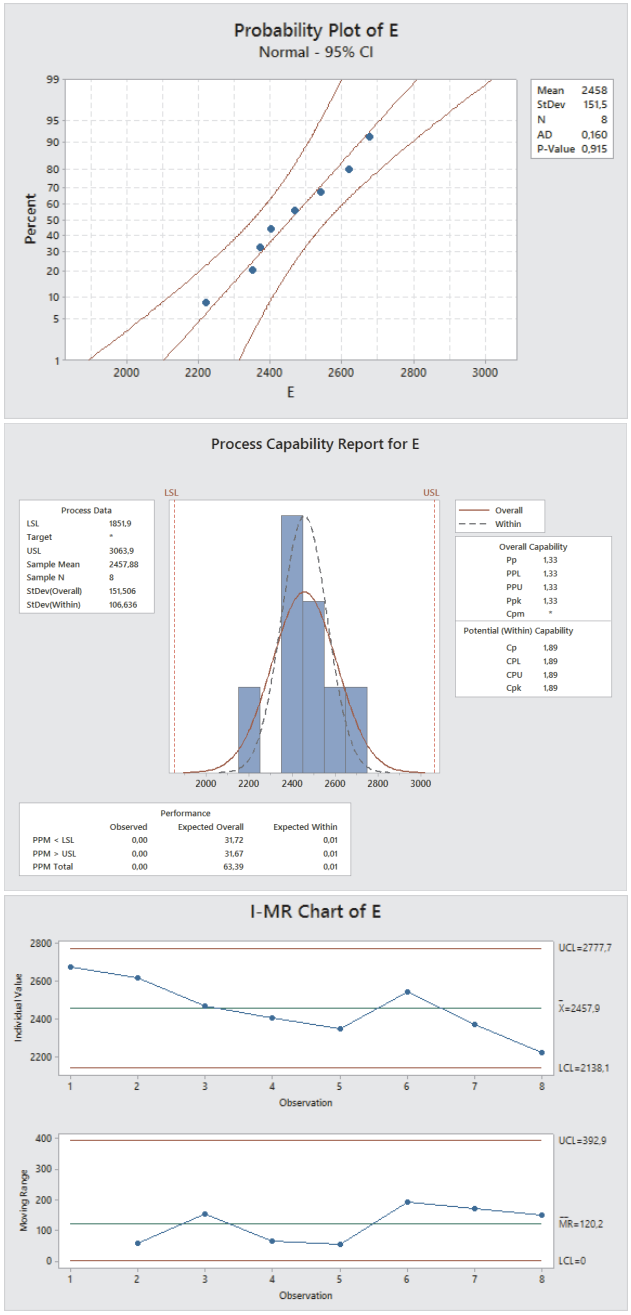

Figure 23: Probability Plot, Process Capability Report and I-MR Chart for the Young modulus E of specimens.

ure 23 is the Probability Plot. Regarding to Young modulus, the specimens have a standard deviation of 151.5, evaluating the overall sample. The data seem to follow approximately the straight line, therefore the Anderson-Darling value is low (0.160) and the P-value is considerably higher than the threshold value. The normal distribution seems to be a good fit for the collected data. From Figure 23 it can be seen that the average value of the measured stiffness is equal to 2457.96N/mm^2 with an interesting data that can be obtained from the estimated percentiles and their confidence intervals. It seems that only the 1% of the values will be placed below the range having as confidence bounds 1852N/mm^2 and 3063N/mm^2 centered in 2457N/mm^2. This feature is interesting because it allows us to obtain a preliminary estimate of the lowest allowable value for the stiffness, useful in design calculations. However, having chosen the sigma level, it was necessary to identify those upper and lower limits which guarantee that the percentage corresponding to the Sigma Level 4 would have fallen within this range. These limits were identified by imposing a P_{pk} (rather than a C_{pk}) equal to 1.33. This approach is more conservative since it allows to take into account the long term variability, statistically more marked than the short one. As indicated, the lower limit for the interval corresponding to the sigma level 4, centered on the mean value, is equal to 1852N/mm^2. This data indicates that at least the 99.38% of the specimens will have a higher modulus of elasticity. This value can be, therefore, used with confidence in the phase of structural optimization of the drone. The last part evaluated in Figure 23 shows that the process is globally stable and performs inside of the limits of acceptance of the Sigma Level 4.

4.2.2 Maximum stress at rupture

The experimental data for the capability analysis are reported in Table 1. The Probability Plot in Figure 24 allows to deduce that the trend is quite linear over the distribution with a sample mean of 35.47N/mm^2 and a standard deviation on the overall sample of 1.41. The p-value is acceptable for our purpose although it is not very high. The second graph shown in Figure 24 reports the process capability and the boundary limits. It can be seen that there is no symmetrical distribution because it is shifted with a maximum towards the higher stress values. The boundary limits with a P_{pk} index equal to 1.33 are 29.85MPa and 41.08MPa. It has to be noted that the ultimate load at which the UAV structure must survive will be the lower limit divided by a safety factor. The control chart in Figure 24 shows a quite randomic trend that will need more specimens to be completely clarified.

4.2.3 Stress at proportional limit

The last extrapolated mechanical data are related to the proportional stress σ_{pro}. It has been calculated as the greatest stress that a material is capable of sustaining without any deviation from the proportionality of stress to

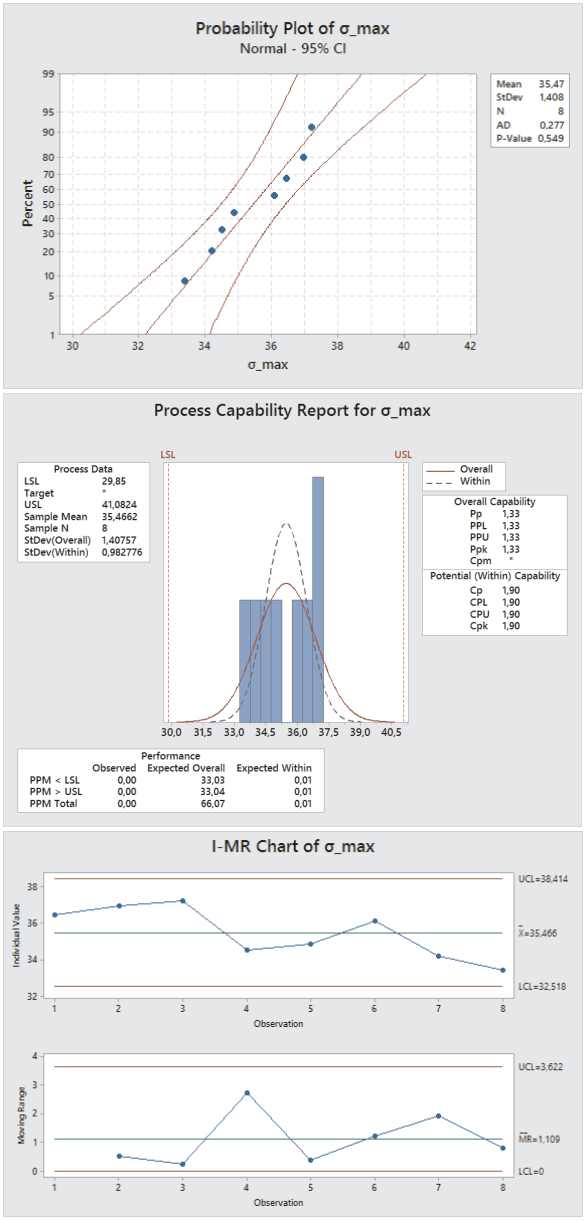

Figure 24: Probability Plot, Process Capability Report and I-MR Chart for the maximum stress at rupture (σ_{max}) of specimens.

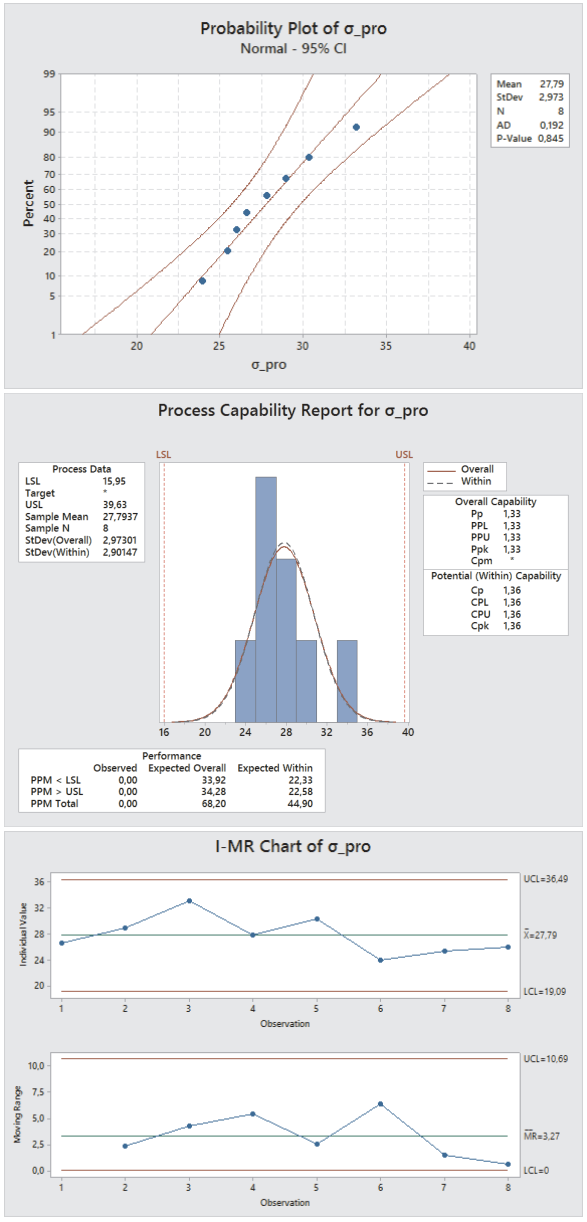

Figure 25: Probability Plot, Process Capability Report and I-MR Chart for the stress at proportional limit (σ_{pro}) of specimens.

strain; it has been conventionally identified in the value of stress at which the coefficient of the linear regression quoted above diverges more than the 5% from the found modulus of elasticity. Results are expressed in N/mm^2. The values recorded for the 8 specimens are reported in Table 1. The Probability Plot is reported in Figure 25 and it shows an almost linear trend with an average value of 27.79MPa, a standard deviation of 2.97 and a p value of 0.85. The Process Capability Report given in Figure 25 shows a symmetrical distribution of the values. In order to be compliant with a Sigma Level of 4, the lower limit was identified in 15.95MPa while the upper limit was 39.63MPa (obtained intersecting the area of the maximum load at rupture of the previous paragraph). The last graph of Figure 25 shows a trend over the different specimens that is randomic and centered over the average value.

5 Conclusions and further improvements

In the proposed work a capability analysis has been set up and preliminary mechanical and dimensional information

have been evaluated to understand if a desktop 3D printer is suitable for the self-production of flying components. It has been proved that almost all the measurements have a good fit with the normal distribution; the boundary limits have been established to have a stable process which performs with a sigma level equals 4. It has been determined that almost all the FDM ABS pieces printed with the present 3D printer will be characterized by a Young Modulus higher than 1851.9MPa, a maximum stress at rupture higher than 29.85MPa and a stress at proportional limit higher than 15.95MPa. These values can be used with confidence as input for a structural analysis. Regarding the dimensional parameters, it has been shown that a scale effect is present on the dimension of the specimens; this feature must be evaluated and corrected into the CAM phase of the construction process. Although, further satisfying analysis must be carried on to understand if the scale effect is constant or if it is related to the dimension of the part.

Acknowledgements

The authors thank Dr. Raffaella Sesana for the assistance with the testing of the specimens and for advices that greatly improved the manuscript. We would also like to show our gratitude to all the members of the PoliDrone team for their support and constant work.

References

[1] Remotely Piloted Aerial Vehicles Issue 2, Italian rules for Civil UAV and RPV, ENAC, Italy, 2016.

[2] The Drone Economy Moves Beyond Science Fiction, Forbes, US, 2015.

[3] S. Brischetto, A. Ciano and A. Raviola, Patent application for industrial invention, A multipurpose modular drone with adjustable arms, registered on 5th November 2015 with temporary number 102015000069620.

[4] C. Ferro, R. Grassi, C. Seclì and P. Maggiore, Additive Manufacturing Offers New Opportunities in UAV Research, 48th CIRP Conference on Manufacturing Systems 2015, Procedia CIRP Vol. 4, 1004–1010, 2016.

[5] Patent for industrial invention, WO2015036907A1, An improved drone structure.

[6] Patent for industrial invention, KR101456035B1, The rotor arm device of multi-rotor type drone.

[7] Patent for industrial invention, WO2004113166A1, Gyropter having increased safety.

[8] Patent for industrial invention, FR2937306A1, Amphibious gyropendular drone for use in e.g. defense application, has safety device arranged in periphery of propulsion device for assuring floatability of drone, and upper propulsion device for maintaining drone in air during levitation.

[9] S.H. Khajavi, J. Partanen and J. Holmstro, Additive manufacturing in the spare parts supply chain, Computers in Industry, 65, 50–63, 2013.

[10] R. Krache and I. Debbah, Some mechanical and thermal properties of PC/ABS blends, Materials Sciences and Applications, Vol. 2, 404–410, 2012.

[11] P.J. Nunez, A. Rivas, E. Garcia-Plaza, E. Beamud and A. Sanz-Lobera, Dimensional and Surface Texture Characterization in Fused Deposition Modelling (FDM) with ABS Plus, The Manufacturing Engineering Society International Conference, MESIC 2015.

[12] B. Vayre, F. Vignat and F. Villeneuve, Designing for Additive Manufacturing, 45th CIRP Conference on Manufacturing Systems 2012, Procedia CIRP Vol. 3, 632–637, 2012.

[13] W. Gao, Y. Zhang, D. Ramanujan, K. Ramani, Y. Chen, C.B. Williams, C.C.L. Wang, Y.C. Shin, S. Zhanga and P.D. Zavattieri, The status, challenges, and future of additive manufacturing in engineering, Computer-Aided Design, Procedia CIRP, 69, 65–89, 2015.

[14] C.C. Kai, G.G.K. Jacob and T. Mei, Interface between CAD and rapid prototyping systems, The International Journal of Advanced Manufacturing Technology, 13, 566–570, 1997.

[15] K.V. Wong and A. Hernandez, A review of additive manufacturing, A International Scholarly Research Network, ISRN Mechanical Engineering, Volume 2012, Article ID 208760, 2012.

[16] L.-C. Zhang, M. Han and S.-H. Huang, An effective error-tolerance slicing algorithm for STL files, The International Journal of Advanced Manufacturing Technology, 20, 363–367, 2002.

[17] K. Lee, Principles of CAD/CAM/CAE Systems, Addison-Wesley Longman Publishing Co., Inc., Boston, MA, USA 1999.

[18] A. Ranellucci, Reprap/Slic3r and the future of 3D printing, Low-cost 3D printings, ICTP, 75–82, 2013.

[19] P. Dudek, FDM 3D printing technology in manufacturing composite elements, Archives of Metallurgy and Materials, 58, 1415–1418, 2013.

[20] R. Singh and S. Singh, Development of nylon based FDM filament for rapid tooling application, The Institution of Engineers, 95, 103–108, 2014.

[21] S. Raut, V. Kumar, S. Jatti, N.K. Khedkar and T.P. Singh, Investigation of the Effect of Built Orientation on Mechanical Properties and Total Cost of FDM Parts, 3rd International Conference on Materials Processing and Characterisation, Procedia Materials Science, 6, 1625–1630, 2014.

[22] ASTM D638-10, Standard Test Method for Tensile Properties of Plastics, Annual Book of ASTM Standards, ASTM International, West Conshohocken, PA, USA, 2010.

[23] S. Ahn, M. Montero, D. Odell, S. Roundy and P. Wright, Anisotropic material properties of fused deposition modeling ABS, Rapid Prototiping, 8, 248–257, 2002.

[24] D. Croccolo, M. De Agostinis and G. Olmi, Experimental characterization and analytical modelling of the mechanical behaviour of fused deposition processed parts made of ABS-M30, Computational Materials Science, 79, 506–518, 2013.

[25] Sharebot srl, Sharebot Next Generation User Manual, 2015.

[26] M. Pincini, Caratterizzazione sperimentale di proprietá meccaniche di componenti costruiti mediante fused deposition modeling, Bachelor degree thesis in Aerospace Engineering discussed at the Politecnico di Torino, Turin, Italy, 2015.

[27] QTest 10, Artisan Technology Group, https://www.artisantg.com/info/PDF__4D54535F51746573745F446174617368656574.pdf, accessed on 27th April 2016.
[28] T.W. Anderson and D.A. Darling, Asymptotic theory of certain "Goodness of Fit" criteria based on stochastic processes, The Annals of Mathematical Statistics, 23, 193–212, 1952.
[29] T.W. Anderson and D.A. Darling, A test of goodness of fit, Journal of the American Statistical Association, 49, 765–769, 1954.
[30] S. Steiner, B. Abraham and J. MacKay, Understanding Process Capability Indices, Institute for Improvement in Quality and Productivity research report, University of Waterloo, Ontario, Canada, 1997.
[31] Minitab, Products, https://www.minitab.com, accessed on 27th April 2016.